SANDIA REPORT
SAND2008-2008
Unlimited Release
Printed April 2008

Flatback Airfoil Wind Tunnel Experiment

Jonathon P. Baker, C.P. “Case” van Dam, and Benson L. Gilbert

Prepared by
Sandia National Laboratories
Albuquerque, New Mexico 87185 and Livermore, California 94550

Sandia is a multiprogram laboratory operated by Sandia Corporation,
a Lockheed Martin Company, for the United States Department of Energy’s
National Nuclear Security Administration under Contract DE-AC04-94AL85000.

Issued by Sandia National Laboratories, operated for the United States Department of Energy by Sandia Corporation.

Available to DOE and DOE contractors from
U.S. Department of Energy
Office of Scientific and Technical Information
P.O. Box 62
Oak Ridge, TN 37831

Telephone: (865) 576-8401
Facsimile: (865) 576-5728
E-Mail: reports@adonis.osti.gov
Online ordering: http://www.osti.gov/bridge

Available to the public from
U.S. Department of Commerce
National Technical Information Service
5285 Port Royal Rd.
Springfield, VA 22161

Telephone: (800) 553-6847
Facsimile: (703) 605-6900
E-Mail: orders@ntis.fedworld.gov
Online order: http://www.ntis.gov/help/ordermethods.asp?loc=7-4-0#online

SAND2008-2008
Unlimited Release
Printed April 2008

Flatback Airfoil Wind Tunnel Experiment

Jonathon P. Baker, C.P. "Case" van Dam, and Benson L. Gilbert
Department of Mechanical and Aeronautical Engineering
University of California
One Shields Avenue
Davis, CA 95616-5294

Dale E. Berg, Sandia National Laboratories Technical Manager

Sandia Contract No. 15890

Abstract

An experimental investigation of blunt trailing edge or flatback airfoils was conducted in the University of California, Davis Aeronautical Wind Tunnel. The flatback airfoil was created by symmetrically adding thickness to both sides of the camber line of a baseline airfoil, while maintaining the maximum thickness-to-chord ratio of 35%. Three airfoils, with geometries based on the baseline airfoil, of various trailing edge thicknesses (0.5%, 8.75%, and 17.5% chord) are discussed in this report. In the present study, each airfoil was tested under free and fixed boundary layer transition flow conditions at Reynolds numbers of 333,000 and 666,000. The fixed transition conditions, used to simulate surface soiling effects, were achieved by placing artificial tripping devices at 2% chord on the suction surface and 5% chord on the pressure surface of each airfoil. The results of this investigation show the blunt trailing edge airfoils reduced the well-documented sensitivity to leading edge transition for thick airfoils. The nominally sharp trailing edge airfoil, with trailing edge thickness of 0.5% chord, performed well under free transition conditions, but the lift characteristics deteriorated significantly when the flow was tripped at the leading edge. As the trailing edge thickness was increased, the effect of leading edge transition diminished, that is, the airfoil lift performance became increasingly similar for free and fixed transition. The flatback airfoils yield increased drag coefficients over the sharp trailing edge airfoil due to an increase in base drag. To address the base drag increment, six different trailing edge devices were investigated for the airfoil with 17.5% chord trailing edge thickness at a Reynolds number of 333,000 under tripped flow conditions. Several of the trailing edge devices caused significant reductions in base drag.

Acknowledgements

This project was supported by TPI Composites of Warren, Rhode Island under Contract 15890 – Revision 4 with Sandia National Laboratories. The primary members of the TPI team were Derek Berry (Principal Investigator) and Steve Nolet of TPI, Kevin Jackson of Dynamic Design, Michael Zuteck of MDZ Consulting and C.P. (Case) van Dam and his students (Jonathon Baker and Benson Gilbert for this particular effort) at the University of California at Davis. The members of the Sandia team were Tom Ashwill, Dale Berg (Technical Manager), Daniel Laird, Mark Rumsey, Herbert Sutherland, Paul Veers and Jose Zayas.

Table of Contents

List of Figures

Introduction

Blunt trailing edge or flatback airfoils have been proposed for the inboard region of large wind turbine blades [1,2,3]. Flatback airfoils provide several structural and aerodynamic performance advantages. Structurally, the flatback increases the sectional area and sectional moment of inertia for a given airfoil maximum thickness [1]. Aerodynamically, the flatback increases the sectional maximum lift coefficient and lift curve slope and reduces the well-documented sensitivity of the lift characteristics of thick airfoils to surface soiling [3].

In the past, many investigations have been conducted on blunt trailing edge airfoils with some of the earliest work by Hoerner [4,5] indicating that the maximum lift-to-drag ratio of thick airfoils can be increased by incorporating a blunt trailing edge, and suggesting application of such airfoils in the blade root region of rotors, such as propellers. Most of these studies simply truncated the trailing edge to achieve the required blunt trailing edge shape, resulting in a reduction in camber and potential loss in lift.

In contrast, the shape of these blunt airfoils seems to be optimal when the trailing edge is thickened, as demonstrated by Standish and van Dam [3]. This results in a reduced adverse pressure gradient on the suction side, thereby creating more lift and mitigating flow separation due to premature boundary-layer transition. Unfortunately, the blunt trailing edge shape also creates a steady or periodic low-pressure flow in the near-wake of the airfoil that gives rise to a drag penalty; perhaps this drag penalty is the reason blunt trailing edges have been largely avoided in the design of subsonic airfoils [6]. Methods to minimize the base drag penalty, including trailing edge splitter plates, trailing edge serrations, base cavities, and trailing edge fairings or wedges, have been investigated for many years. The literature on these trailing edge modifications has been studied and the main findings are presented in a previous report by van Dam and Kahn [7].

Limited experimental data are available that validate the aerodynamic performance benefits of the blunt trailing edge concept for thick airfoils. This lack of experimental data in the open literature prompted a wind tunnel study of a thick blade section with a blunt trailing edge. In the present study, three airfoils with trailing edge thicknesses ranging from 0.5% to 17.5% chord were experimentally analyzed under free and fixed transition conditions. To address the base drag increment, six different trailing edge devices were affixed to the airfoil with 17.5% chord trailing edge thickness. In the following sections, the three airfoils, six trailing edge devices, and the corresponding wind tunnel results are presented.

Airfoils and Trailing Edge Devices

Airfoils

The FB airfoil series, presented in the final report of Phase I of the Blade System Design Study (BSDS) [2], was selected for experimental investigation. This series of airfoil shapes was generated by combining a low-pressure side shape drawn from the thick, high lift inboard NREL

airfoils, and a structurally efficient high-pressure side drawn from the LS–1 series airfoils. Figure 1 depicts the FB3500-0050 airfoil, the baseline airfoil with a nominally sharp trailing edge. The actual trailing edge thickness-to-chord ratio of this airfoil is not zero but 0.5%. The reasons for the finite trailing edge thickness are twofold: 1) physically, any blade section or wind tunnel model will have a finite trailing edge thickness and it is good practice to incorporate this attribute in the design and analysis from the onset; 2) computationally, different grid topologies are required for zero and finite trailing edge thickness airfoils. Using a small, finite trailing edge thickness allows for the sharp trailing edge airfoil to be analyzed using the same grid type as the blunt trailing edge airfoils, thus facilitating comparison of computational results.

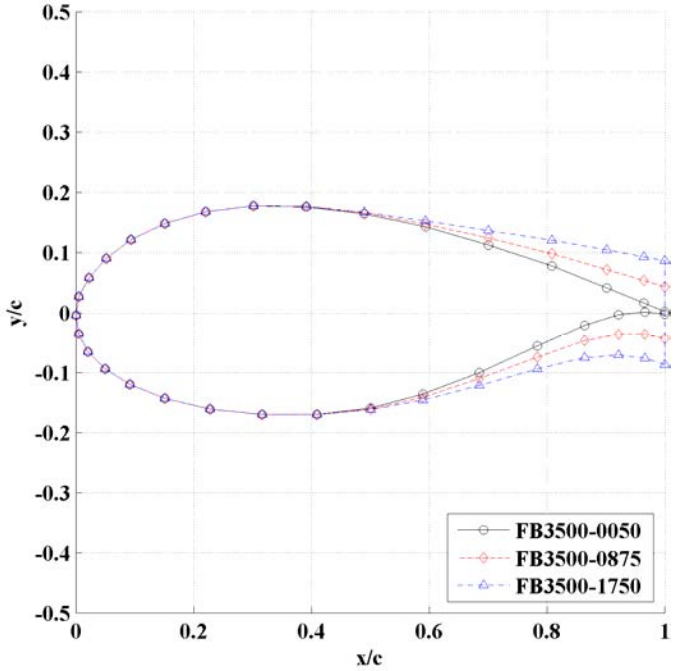

Figure 1. Blade section geometries for the baseline FB3500-0050 airfoil and its derivative flatback airfoil sections: FB3500-0875 and FB3500-1750.

The FB3500-0875 airfoil has the identical maximum thickness as the FB3500-0050 airfoil but has a trailing-edge thickness of 8.75%, as shown in Figure 1. Note that the FB3500-0875 airfoil with its maximum thickness-to-chord ratio (t/c) of 35% and trailing edge thickness-to-chord ratio (t_{te}/c) of 8.75% closely resembles the FB3423-0596 (t/c = 34.23% and t_{te}/c = 5.96%) section shape investigated in BSDS Phase I [2]. The blunt trailing edge was created by symmetrically adding thickness to either side of the camber line of the FB3500-0050 airfoil using an exponential blending function to smoothly distribute the increased thickness along the chord.

The FB3500-1750 airfoil has the identical maximum thickness as the FB3500-0050 and the FB3500-0875 airfoils but has a trailing-edge thickness of 17.5% as shown in Figure 1. The results of this paper will show, by using the flatback concept, a sharp trailing edge airfoil of this thickness (35%) can be modified to have lift characteristics that are largely insensitive to surface soiling. A simple design guideline for blunt trailing edge or flatback airfoils is to limit the difference between maximum thickness-to-chord ratio and trailing edge thickness-to-chord ratio

to approximately 20% to make surface insensitive lift characteristics achievable. Based on this rule-of-thumb one would expect to see significant sensitivity to surface soiling for the FB3500-0050 and FB3500-0875 airfoils, but little or no sensitivity for the FB3500-1750 airfoil.

Trailing Edge Devices

The addition of trailing edge modifications is proposed to alleviate the base drag of the FB3500-1750 airfoil (see Figure 1). The trailing edge modifications used in the present study consist of metal plates which were attached to the trailing edge of the FB3500-1750 airfoil model. The plates were manufactured in an L-shape such that they could be mounted perpendicular to the flat part of the trailing edge. The splitter plates were designed to extend 17.5% chord (identical to the trailing edge thickness) from the trailing edge. Three splitter plate edge treatments were investigated, including a non-serrated edge and splitter plates with 60º and 90º edge serrations as shown in Figure 2. The manufacturing specifications for the splitter plates are provided in the appendix.

The splitter plates were arranged on the trailing edge in two configurations. The first configuration involved mounting a single plate at the centerline of the trailing edge of the airfoil. The second configuration consisted of two plates mounted at the limits of the trailing edge, forming a base cavity. The first and second configurations will be referred to as single splitter plate and double splitter plate, respectively. Six splitter plates were manufactured to allow for the investigation of the two configurations (single plate and double plates) with three different edge treatments.

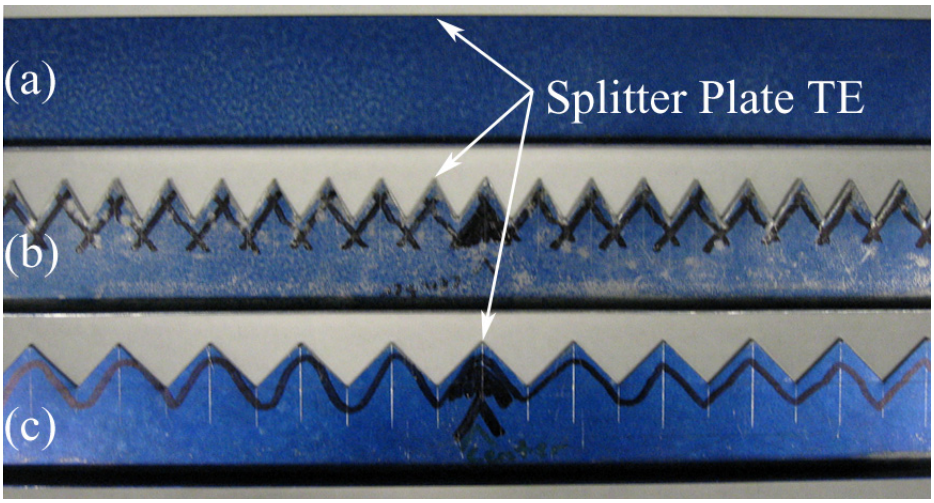

Figure 2. (a) Non-serrated, (b) 60º-serrated, and (c) 90º-serrated splitter plate edge treatments. The trailing edge of the splitter plate is noted.

Experimental Methods

The aeronautical wind tunnel (AWT) at UC Davis is an open circuit, low turbulence wind tunnel manufactured by Aerolab [8]. A schematic diagram of the wind tunnel is offered in Figure 3. The wind tunnel has test section cross-sectional dimensions of 0.86 m × 1.22 m (2.8 ft × 4.0 ft) and length of 3.66 m (12.0 ft). The test section is constructed with parallel sides, utilizing four

tapered fillets to compensate for boundary layer growth and to preserve constant pressure throughout the section. The wind tunnel has low turbulence levels, less than 0.1% full scale (FS), for the initial 80% of the test section. These low turbulence levels are ensured by the tunnel inlet, which houses an aluminum honeycomb screen and four anti-turbulence screens to reduce vorticity as the flow enters the tunnel. The wind tunnel is driven by a Reliance Electric, Premium Efficient 125 hp motor and a Joy size 84-26-FB-1000 Arrangement 4 direct drive Axivane vaneaxial fan. The velocity setting of the fan can be controlled to within ±0.2% FS by an electronic speed controller (Mitsubishi Meltrac A-100 variable frequency drive).

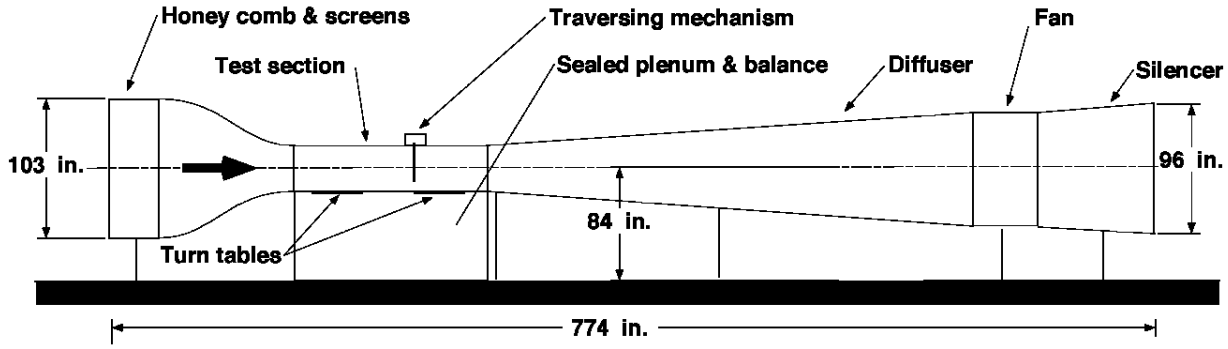

Figure 3. Schematic of the UCD Aeronautical Wind Tunnel.

The wind tunnel test section contains two 0.91 m (36.0 in.) diameter turntables for the mounting of test apparatus. For a two-dimensional (2D) airfoil experiment, an airfoil model is placed over the first turntable and fixed to a six-component pyramidal balance such that the model bisects the test section vertically and extends from the floor to the ceiling (see Figure 4). In the present study, the balance was used to measure lift and pitching moment about the quarter chord. Drag was measured using a wake traverse method [9].

Figure 4. A two-dimensional airfoil model, mounted in the UCD AWT test section.

The experimental analysis was conducted for the FB3500-0005, FB3500-0875, and FB3500-1750 airfoils shown in Figure 1. Each airfoil model was constructed to have a 0.203 m (8.0 in.) chord and a 0.8382 m (33 in.) span. The experiments were conducted for Reynolds numbers of 333,000 and 666,000 for free and fixed transition. Fixed transition was attained using 0.25 mm

(0.01 in.) thick zigzag trip-tape placed at 2% and 5% chord, measured from the leading edge of the airfoil to the leading edge of the trip-tape, on the suction and pressure surfaces, respectively.

The FB3500-1750 airfoil was modified by affixing splitter plates to the trailing edge using the two configurations and three edge treatments described above. Each splitter plate was mounted perpendicular to the trailing edge of the airfoil using four bolts fastened to threaded inserts in the model (see Figure 5). Tape was applied to the splitter plate to seal the junction of the splitter plate and the trailing edge.

Figure 5. The FB3500-1750 airfoil model, with single 90º-serrated plate, mounted in the UCD AWT test section.

A maximum thickness-to-chord ratio (t/c) of 35% was selected for this experiment because it is at the high end of section shape thickness considered for the root region of wind turbine blades. One of the problems with wind tunnel testing thick airfoils is that these types of models tend to create a significant amount of solid blockage (ratio of frontal area of the model to the test section cross-sectional area) and wake blockage (size of model wake relative to that of test section), thereby affecting the flow development in the wind tunnel test section. Good engineering practice keeps solid blockage at 5% or less, but this value limits the model chord length, which in turn limits attainable chord Reynolds numbers [10].

The model selection for this study led to a solid blockage ratio of 6% (model maximum thickness of 0.071 m and test section width of 1.22 m). A series of computational fluid dynamics simulations were conducted by van Dam, Mayda, and Chao [11] to emulate the application of standard wind tunnel wall corrections [10] to the test results for flatback airfoil models similar to those investigated here. These simulations indicate that standard corrections are nominally valid for flatback airfoils up to 40% maximum thickness-to-chord ratio, with solid blockage ratios of up to 10%. Thus, all data presented in this report are corrected for wind tunnel wall effects using methods presented in Barlow et al. [10].

Results and Discussion

Flatback Airfoil Analysis

The aerodynamic characteristics of the FB3500-0050 airfoil are presented in Figs. 6–8. The FB3500-0050 airfoil has t/c = 35% and t_{te}/c = 0.5%. Due to the large maximum thickness and small trailing edge thickness, leading edge surface roughness sensitivity was expected and this sensitivity is clearly shown in Figure 6. Under free transition conditions, the FB3500-0050 airfoil behaved like a typical airfoil in that it has a nominally linear lift curve slope prior to stall, which occurred at approximately 19º. With transition fixed near the leading edge, however, the airfoil behaved in a completely different manner. In this case, the airfoil generated positive lift for all incidence angles, but with stall behavior occurring near -2º. Beyond 2º, the angle of minimum post-stall lift, lift increased with increasing angle of attack at a much reduced lift curve slope, compared to free transition conditions, indicative of separated flow with flat plate lift effects. These characteristics were found for both Reynolds numbers investigated.

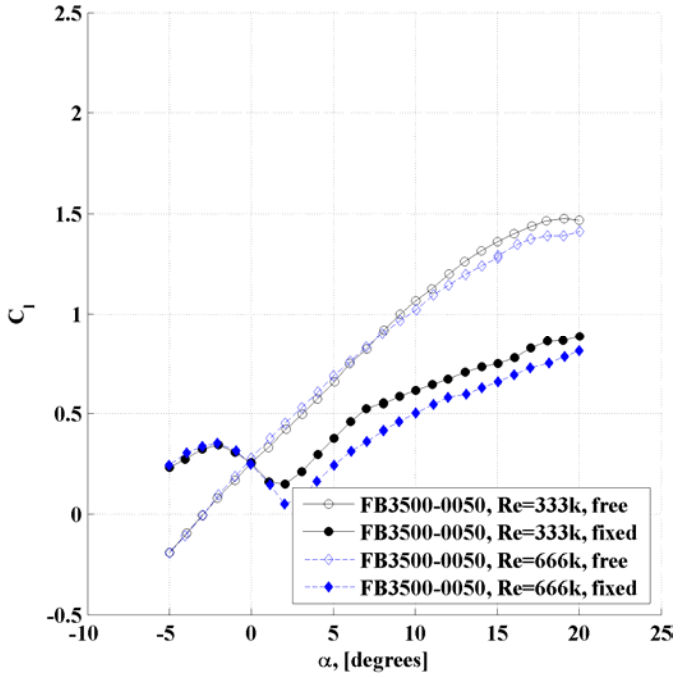

Figure 6. Measured lift curves for FB3500-0050 airfoil with transition free and fixed at Reynolds numbers of 333,000 and 666,000.

The pitching moment characteristics of the FB3500-0050 airfoil are shown in Figure 7. The free transition pitching moment was stable and nose down for all incidence angles. For the fixed transition cases, the boundary layer transition sensitivity is clearly demonstrated by the pitching moment instability for angles of incidence between -5º and 1º. In fact, between 1º and 5º incidence, the airfoil had a slight nose-up pitching moment at Re = 666,000.

The drag characteristics for the FB3500-0050 airfoil are shown in Figure 8. Comparison of free and fixed transition at the same Reynolds number shows fixed transition dramatically increased the drag. For example, under free transition at Re = 666,000, the drag coefficient increased from

0.0151 at 0º to 0.0673 at 16º. Under fixed transition at the same Reynolds number, the drag coefficient increased from 0.0290 at 0º to 0.1756 at 16º.

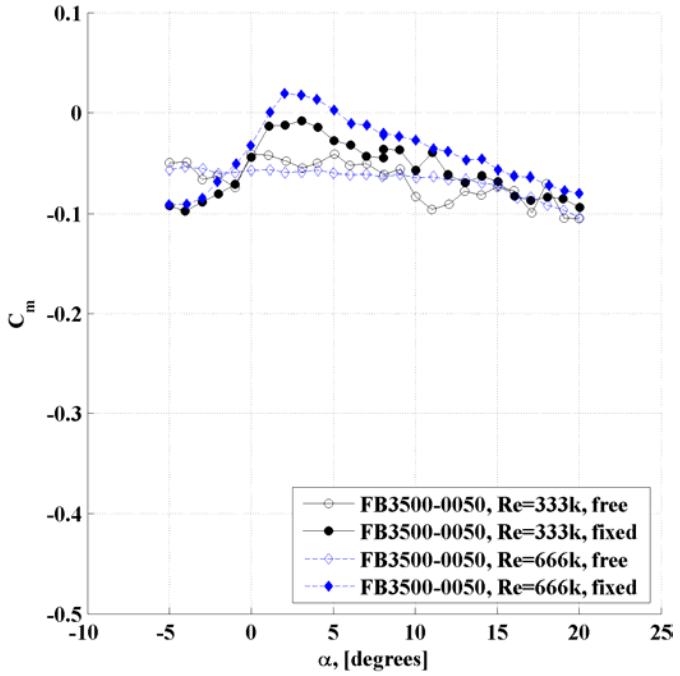

Figure 7. Measured pitching moment curves for FB3500-0050 airfoil with transition free and fixed at Reynolds numbers of 333,000 and 666,000.

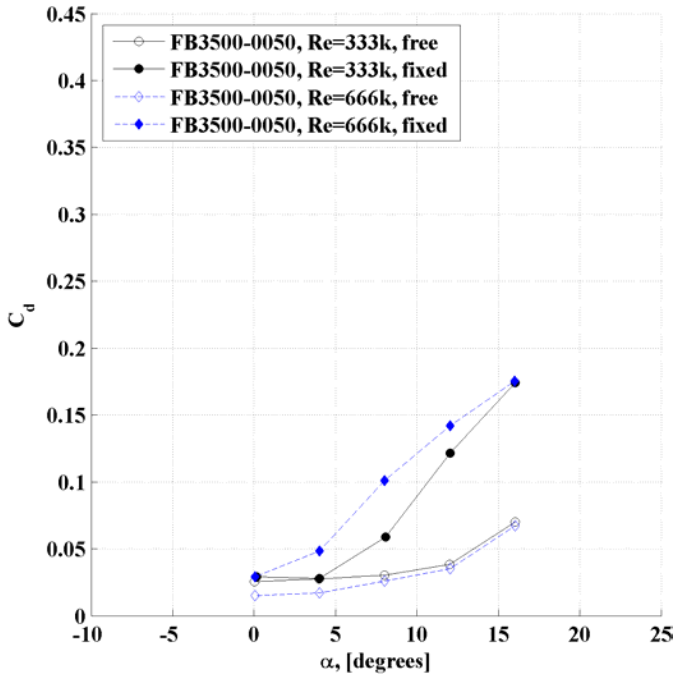

Figure 8. Measured drag curves for FB3500-0050 airfoil with transition free and fixed at Reynolds numbers of 333,000 and 666,000.

The results for the FB3500-0875 airfoil are shown in Figs. 9–11. The FB3500-0875 airfoil has t/c = 35% and t_{te}/c = 8.75%. The lift characteristics of this airfoil are shown in Figure 9. The FB3500-0875 airfoil was clearly influenced by leading edge transition conditions. However, the sensitivity of this airfoil's lift characteristics to surface roughness in the leading edge region was dramatically diminished when compared to the FB3500-0050 airfoil, as shown in Figure 6. In fact, the free and fixed transition cases for the FB3500-0875 airfoil had nearly identical lift curve slopes until the fixed transition cases stalled at around 6º. In contrast, free transition stall occured at approximately 13º and 15º for Reynolds numbers of 666,000 and 333,000, respectively. The fixed transition FB3500-0875 airfoil also behaved differently from the free transition case at angles of incidence less than 2º. At these angles of incidence, the fixed transition lift curve slopes were less than the free transition counterparts.

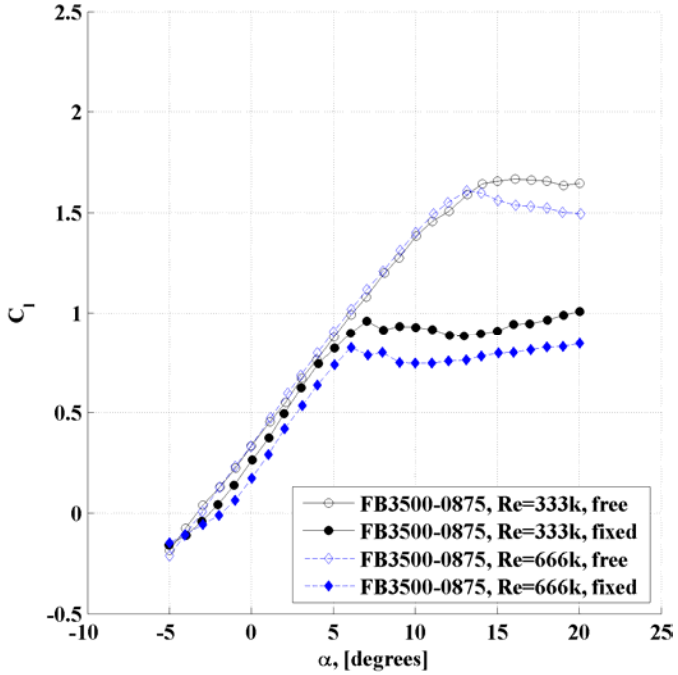

Figure 9. Measured lift curves for FB3500-0875 airfoil with transition free and fixed at Reynolds numbers of 333,000 and 666,000.

As shown in Figure 10, the pitching moment characteristics do not appear to be significantly affected by changes in the transition location. For all four cases analyzed, the FB3500-0875 airfoil had stable nose-down pitching moment for all angles of incidence.

The drag results for the FB3500-0875 airfoil are presented in Figure 11. The fixed transition cases exhibited an increase in drag over the free transition counterparts. For instance, at 16º and Re = 666,000, the fixed transition case produced 625 more drag counts than the corresponding free transition case.

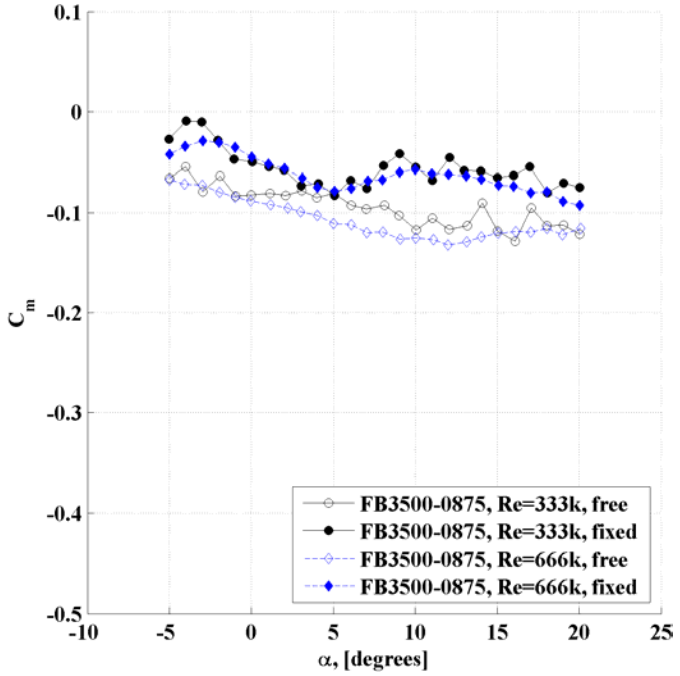

Figure 10. Measured pitching moment curves for FB3500-0875 airfoil with transition free and fixed at Reynolds numbers of 333,000 and 666,000.

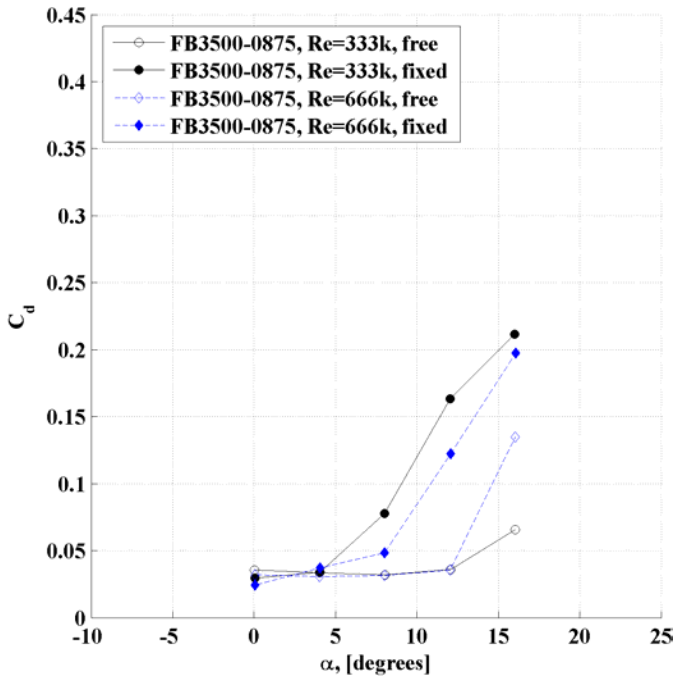

Figure 11. Measured drag curves for FB3500-0875 airfoil with transition free and fixed at Reynolds numbers of 333,000 and 666,000.

The experimental results for the FB3500-1750 airfoil are shown in Figs. 12–14. The FB3500-1750 airfoil has t/c = 35% and t_{te}/c = 17.5%. The lift characteristics of this airfoil are shown in Figure 12. The lift characteristics of the free and fixed transition cases were nearly identical except for an earlier onset of stall for the fixed transition. When transition was fixed near the leading edge, the airfoil stalled precipitously at around 12º. The free transition case stall was less dramatic and was delayed until 19º and 20º for Reynolds numbers of 666,000 and 333,000, respectively.

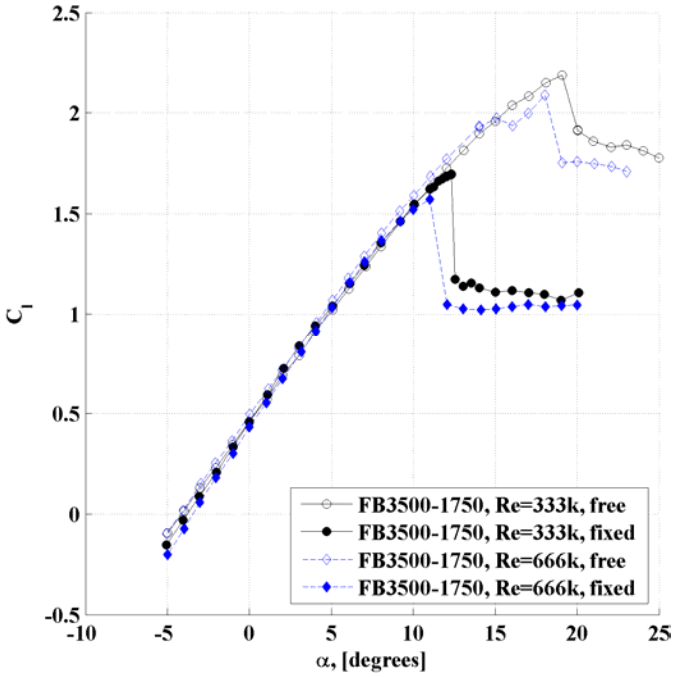

Figure 12. Measured lift curves for FB3500-1750 airfoil with transition free and fixed at Reynolds numbers of 333,000 and 666,000.

The FB3500-1750 airfoil had similar pitching moment characteristics as the FB3500-0875 airfoil, as shown in Figure 13. Each of the four cases tested was positively stable and the pitching moment varied nearly linearly for angles of incidence below stall. The pitching moment did increase slightly for free and fixed transition post-stall, but remained nose-down.

The drag characteristics of the FB3500-1750 airfoil are shown in Figure 14. For the fixed transition cases, the drag increased significantly for angles of incidence at or above stall. For example, for Reynolds numbers of 666,000 at 16º, the drag coefficient was 0.1043 and 0.3833 for free and fixed transition, respectively.

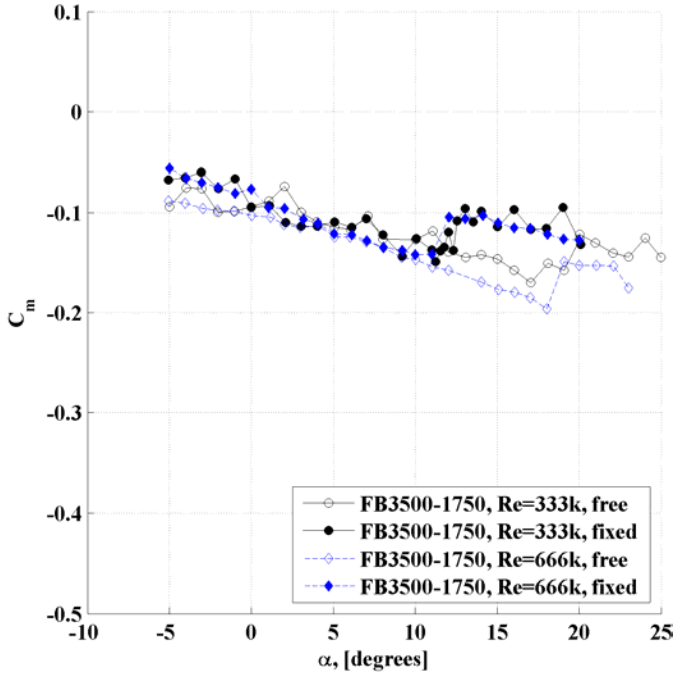

Figure 13. Measured pitching moment curves for FB3500-1750 airfoil with transition free and fixed at Reynolds numbers of 333,000 and 666,000.

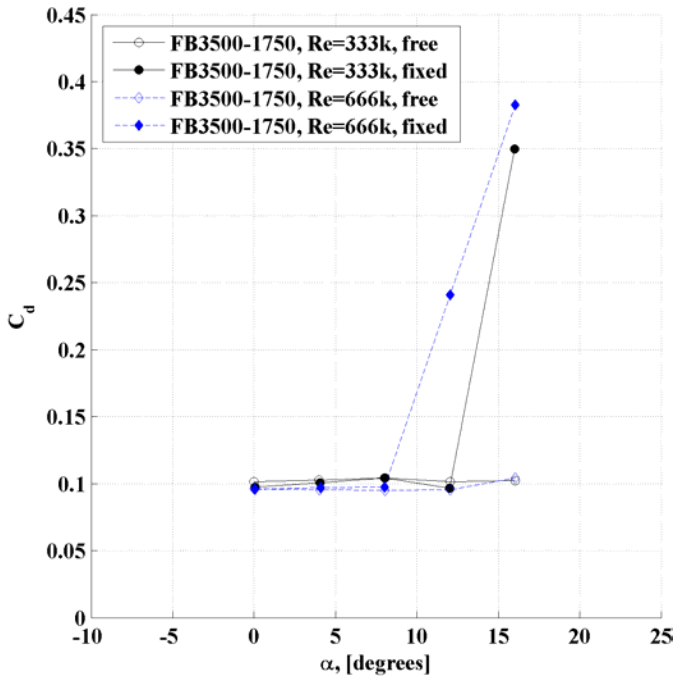

Figure 14. Measured drag curves for FB3500-1750 airfoil with transition free and fixed at Reynolds numbers of 333,000 and 666,000.

The sensitivity of the lift characteristics of the FB3500-0050 airfoil to surface soiling is believed to be due to the steep adverse pressure gradient in the pressure recovery region of the airfoil. Under fixed transition conditions, the flow over the suction surface of the airfoil was separated over most of the angle–of–attack range. This is in contrast to the free transition conditions, when the flow over the suction surface was mostly attached, as demonstrated by the much steeper lift curve slope seen in Figure 6. The leading-edge surface roughness sensitivity can be reduced by "opening up" the trailing edge of the airfoil, by adding symmetrical thickness to the pressure and suction surfaces of the airfoil about the camber line, to create a flatback airfoil. The sensitivity reduction is achieved by reducing the adverse pressure gradient on the suction surface of the airfoil and allowing some of the pressure recovery to occur off-body, i.e. in the wake of the airfoil. This reduction in surface soiling sensitivity was found for the FB3500-0875 airfoil and to a greater extent for the FB3500-1750 airfoil, which have trailing edge thicknesses of 8.75% and 17.5%, respectively. To demonstrate this more clearly, a comparison of the aerodynamic characteristics of the flatback airfoils and the nominally sharp trailing edge airfoil is presented below.

Figures 15 and 16 show a comparison of the lift and drag characteristics for the FB3500-0050 and FB3500-0875 airfoils, under free and fixed transition conditions at Re = 666,000. Under free transition conditions, the lift benefits (Figure 15) of the FB3500-0875 airfoil compared to the FB3500-0050 are counterbalanced by the drag penalty the blunt trailing edge created (Figure 16). Specifically, Figure 15 shows a notable difference in the lift characteristics of the airfoils; the FB3500-0875 airfoil achieved a maximum lift coefficient of 1.61 at approximately 13º, while the FB3500-0050 airfoil was able to produce a maximum lift coefficient of 1.39 before stalling at around 19º. Figure 16 shows the free transition drag of the FB3500-0875 airfoil was greater than the FB3500-0050 by up to approximately 110% prior to stall.

Under fixed transition, the advantages of the flatback airfoils become evident. Figure 15 shows the fixed transition FB3500-0875 airfoil was able to maintain attached flow until around 6º, while the fixed transition FB3500-0050 airfoil stalled at around -2º. In addition, the lift slope of the fixed transition FB3500-0875 airfoil closely resembled its free transition counterpart prior to stall. This is in contrast to the fixed transition FB3500-0050 airfoil lift curve, which did not resemble the free transition FB3500-0050 airfoil lift curve at all. The fixed transition drag curves for these airfoils were similar, as shown in Figure 16. At this condition, however, the FB3500-0875 airfoil yielded lower drag for incidence angles less than 16º.

Figures 17 and 18 show a comparison of the FB3500-0050 and FB3500-1750 airfoils, under free and fixed transition conditions at Re = 666,000. By increasing the trailing edge thickness from 8.75% to 17.5% chord, the leading edge roughness sensitivity was further reduced. The FB3500-1750 airfoil at fixed transition conditions not only stalled much later than the FB3500-0050 and FB3500-0875 airfoils, but also its behavior was nearly identical to the free transition case, up to incidence angles of 11º for lift and 8º for drag, as shown in Figs. 17 and 18, respectively. While the stall for this airfoil (both free and fixed transition) was the most abrupt, the lift curve slope of the FB3500-1750 airfoil was nearly unaffected by transition condition. Also, notice the high maximum lift coefficients of the FB3500-1750 airfoil, which were around 2.09 and 1.58 for free and fixed transition, respectively. In contrast, the free transition FB3500-0050 airfoil maximum lift coefficient was only 1.39. Figure 18 shows the FB3500-1750 airfoil

consistently produced more drag than the sharp trailing edge airfoil, probably due in large part to an increase in base drag.

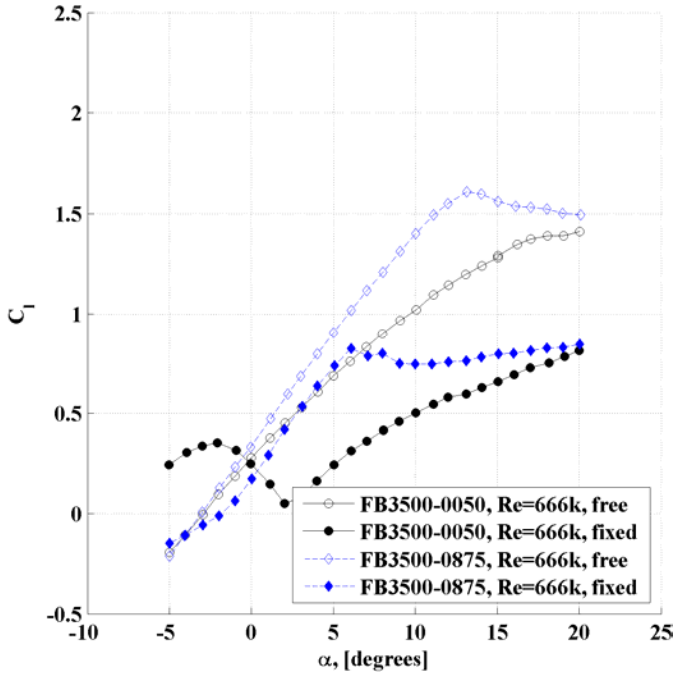

Figure 15. Comparison of lift characteristics of the FB3500-0050 and FB3500-0875 airfoils, transition free and fixed at Re = 666,000.

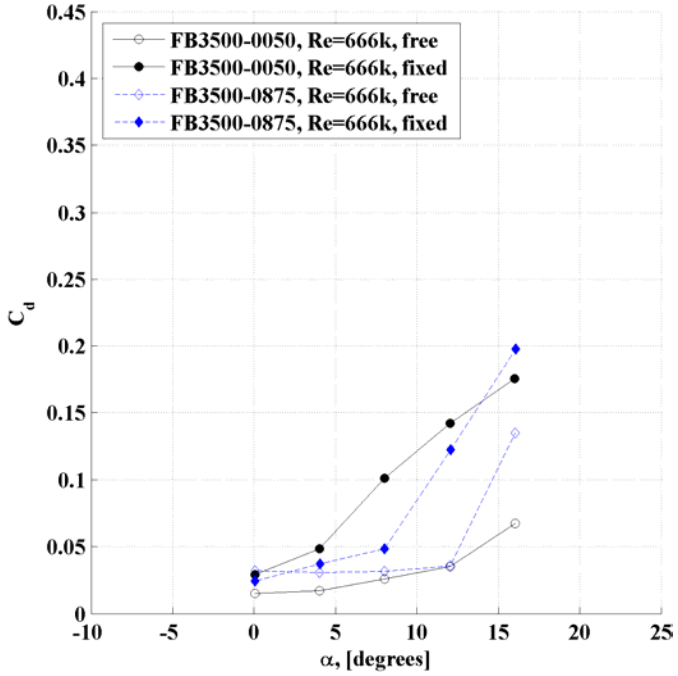

Figure 16. Comparison of drag characteristics of the FB3500-0050 and FB3500-0875 airfoils, transition free and fixed at Re = 666,000.

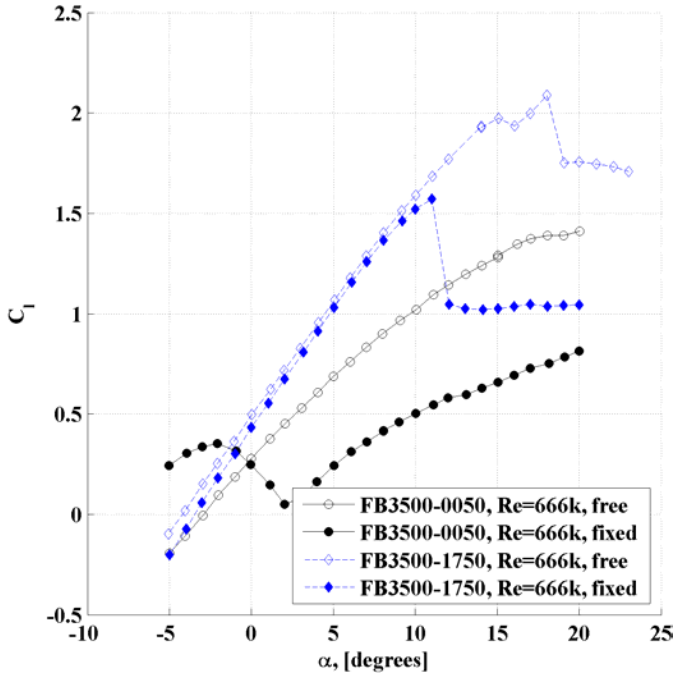

Figure 17. Comparison of lift characteristics of the FB3500-0050 and FB3500-1750 airfoils, transition free and fixed at Re = 666,000.

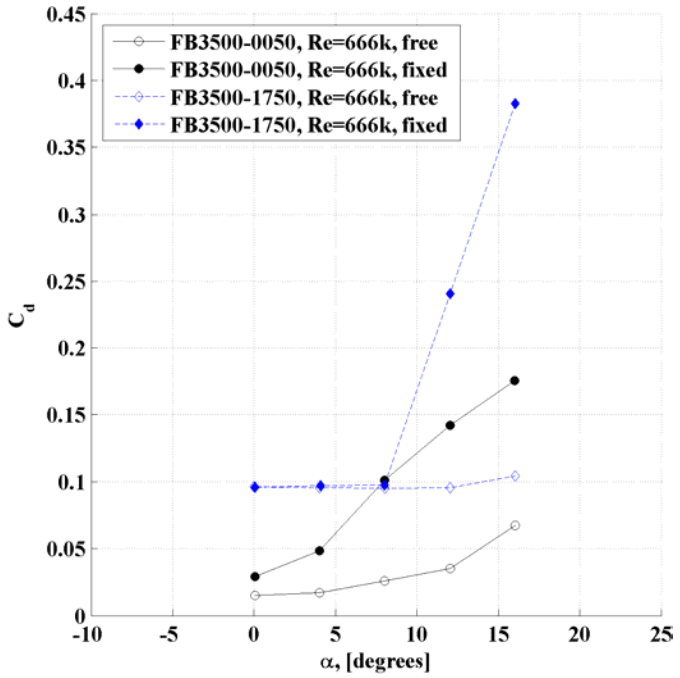

Figure 18. Comparison of drag characteristics of the FB3500-0050 and FB3500-1750 airfoils, transition free and fixed at Re = 666,000.

Effect of Trailing Edge Modifications

The effects of the trailing edge modifications for the FB3500-1750 at a chord Reynolds number of 333,000 under fixed and free conditions are presented in Figs. 19 and 20. The resulting lift curves are presented in Figures 19a and 19b for the single and double splitter plate configurations, respectively. Figure 19a shows that the single splitter plate configuration did not significantly affect the airfoil lift characteristics in the linear regime, though there was some loss in maximum lift and a reduction of the stalling incidence angle. The single non-serrated splitter plate resulted in the largest loss in maximum lift coefficient and reduction in stall angle. The two serrated, single splitter plates caused nearly identical maximum lift and stalling angle of incidence.

Figure 19b presents the lift results for the double splitter plate configurations. When compared to baseline, the double splitter plate configurations resulted in an increased lift curve slope and an increase in zero lift angle of incidence (α_0). The increased α_0 is likely the result of an effective change in airfoil camber due to the addition of the splitter plates as extensions from the suction and pressure surfaces, perpendicular to the trailing edge. Since the trailing edge was set perpendicular to the chord line, and not the mean (camber) line, the splitter plates in this configuration act to reduce the camber, similar to a flap deflected upward. The increase in the lift curve slope is likely due to the additional chord length afforded by the splitter plates. As mentioned previously, the splitter plates were designed to be the same length as the trailing edge thickness, or 17.5% chord. Thus, the addition of the double splitter plates effectively increased the chord of the airfoil by 17.5%. The reduced camber and increased chord effects were not found for the single splitter plate configuration (Figure 19a), likely due to the location of the single splitter plate immersed in the separated wake of the airfoil.

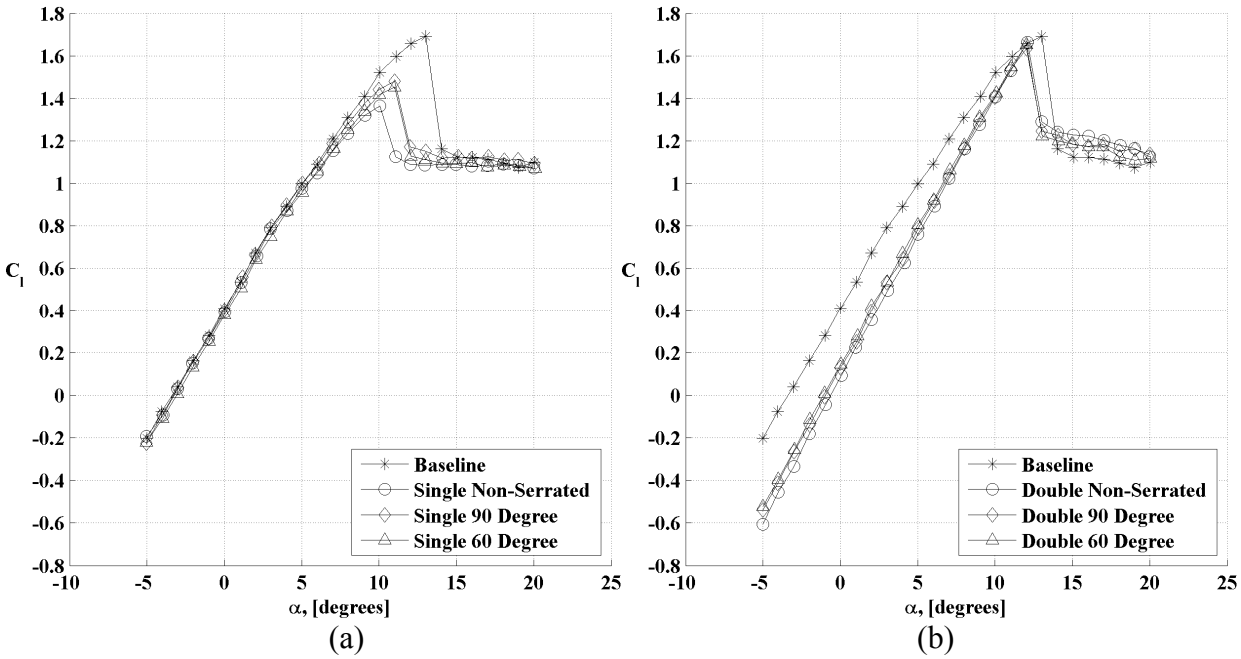

Figure 19. Measured lift curves for the FB3500-1750 airfoil with fixed transition at a Reynolds number of 333,000: (a) single splitter plate configuration, (b) double splitter plate configuration.

The splitter plates demonstrate significant drag reduction capabilities as shown in Figure 20. Figure 20a indicates the single splitter plate reduced the drag by nearly 50% for low angles of attack. As the angle of attack increased, this reduction in drag diminished slightly until the airfoil stalled.

Compared to the single splitter plate configuration, the double splitter plate was not as effective at mitigating drag, as shown in Figure 20b. The maximum drag reduction for all of the double splitter plate cases was approximately 25% for the double splitter plate with 60º-serrated edge treatment at 8º. In general, drag reduction improved for the double splitter plate configuration with increasing incidence angles. While splitter plate edge treatments did not seem to have significant effect for the single splitter plate configuration, the same cannot be said for the double splitter configuration. With double splitter plates, the 60º-serrated edge performed most effectively, followed by the 90º-serrated edge and the non-serrated edge, respectively.

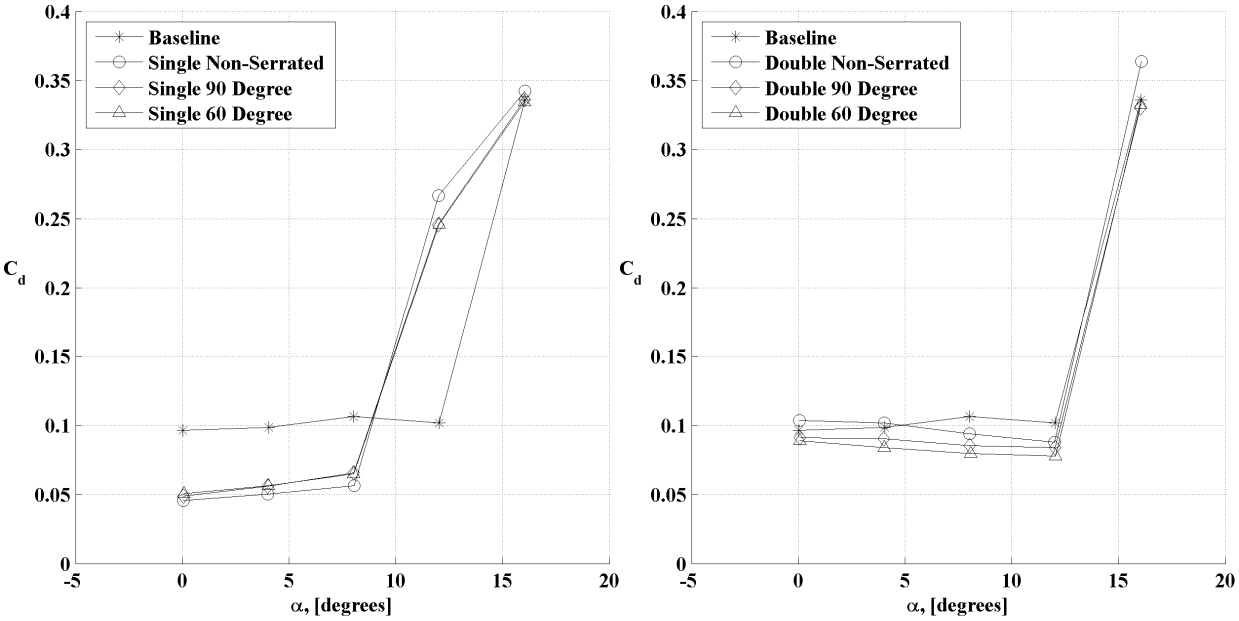

Figure 20. Measured drag curves for the FB3500-1750 airfoil with fixed transition at a Reynolds number of 333,000: (a) single splitter plate configuration, (b) double splitter plate configuration.

During testing, a low amplitude, high frequency noise was observed to occur between incidence angles of 5º and 9º when splitter plates were attached to the FB3500-1750 airfoil trailing edge. The frequency of the noise was nearly constant for all of the splitter plate configurations. The noise amplitude was most affected by splitter plate configuration and somewhat less affected by edge treatment. The noise amplitude was largest for the double splitter plate configuration, with the 60º-serrated plates producing the largest amplitude, the 90º-serrated plates producing slightly less amplitude, and the non-serrated plates producing the lowest amplitude noise. Thus, the double splitter plate with 60º-serrated edge had the largest amplitude and the single splitter plate with non-serrated edge had the smallest amplitude.

Conclusions

The aerodynamic characteristics of a flatback airfoil series have been analyzed in the University of California, Davis Aeronautical Wind Tunnel. The flatback airfoil is created by adding thickness symmetrically about the camber line of a sharp trailing edge airfoil. The baseline FB3500-0050 airfoil is a nominally sharp trailing edge thickness airfoil with an actual trailing edge thickness of 0.5% chord. The FB3500-0875 and FB3500-1750 airfoils are flatback airfoils with 8.75% and 17.5% chord trailing edge thicknesses, respectively. The sensitivity of the FB3500-0050 airfoil to surface roughness was demonstrated in the early onset of flow separation when the boundary layer was tripped near the leading edge. The sensitivity is due to the steep adverse pressure gradient present on the upper surface in the pressure recovery region of thick airfoils such as the FB3500. The flatback airfoils deferred some of the pressure recovery to the wake of the airfoil, thereby reducing the on-surface adverse pressure gradient and reducing the leading edge roughness sensitivity. The flatback airfoils tended to incur greater drag penalties, due in large part to the addition of base drag.

In order to mitigate base drag, single and double splitter plates were applied to the FB3500-1750 airfoil. For both configurations, three edge treatments, including non-serrated, 90º-serrated, and 60º-serrated edges, were investigated. Drag reductions of as much as 50% were achieved using the single splitter plate configuration; these reductions diminished slightly with increasing angle of incidence. The single splitter plate minimally affected lift performance, causing only a slight reduction of the lift curve slope and stall angle of attack. Serrations to the plate edge in the single splitter plate configuration had little effect on lift and drag.

The double splitter plate configuration caused drag reductions of up to 25% compared to baseline; these reductions increased slightly with increasing angle of incidence. The double splitter plate configuration caused increases in the lift curve slope and zero lift angle of attack of the FB3500-1750 airfoil. The increased lift curve slope is likely due to the increased chord length of the airfoil created by the addition of the double splitter plates. The increased zero lift angle of attack is likely due to an effective reduction in camber caused by mounting the double splitter plates perpendicular to the trailing edge (parallel to the chord line) of the airfoil. These phenomena were not observed for the single splitter plate configuration due to separated flow surrounding the entire plate. In the double splitter plate configuration, however, the flow surrounding the plate is not necessarily detached on all surfaces. In future investigations, perhaps this decrease in camber can be mitigated by aligning double splitter plates with the camber line of the airfoil, or by matching the slope of the suction and pressure surfaces. For the double splitter plate configuration, serrations on the downstream edge of the splitter plates caused improved performance compared to a non-serrated edge.

References

1 TPI Composites, "Innovative Design Approaches for Large Wind Turbine Blades," SAND2003-0723, Sandia National Laboratories, Albuquerque, NM, Mar. 2003.

2 TPI Composites, "Innovative Design Approaches for Large Wind Turbine Blades – Final Report," SAND2004-0074, Sandia National Laboratories, Albuquerque, NM, May 2004.

3 Standish, K.J., and van Dam, C.P., "Aerodynamic Analysis of Blunt Trailing Edge Airfoils," Journal of Solar Energy Engineering, Vol. 125, Nov. 2003, pp. 479-487.

4 Hoerner, S.F., "Base Drag and Thick Trailing Edges," Journal of the Aeronautical Sciences, Vol. 17, No. 10, Oct. 1950, pp. 622-628.

5 Hoerner, S.F., *Fluid-Dynamic Drag*, Hoerner Fluid Dynamics, Bricktown, NJ, 1965.

6 Nash, J., "A Review of Research on Two-Dimensional Base Flow," ARC R&M No. 3323, Aeronautical Research Council, 1963.

7 van Dam, C.P., and Kahn, D.L., "Trailing Edge Modifications for Flatback Airfoils," SAND2008-1781, Sandia National Laboratories, Albuquerque, NM, March 2008.

8 Aerolab, Operating Handbook for the UC Davis Low Turbulence Tunnel.

9 Baker, J.P., Standish, K.J., and van Dam, C.P., "Two-Dimensional Wind Tunnel and Computational Investigation of a Microtab Modified Airfoil," Journal of Aircraft, Vol. 44, No. 2, 2007, pp. 563-572.

10 Barlow, J.B., Rae, W.H., and Pope, A., Low-Speed Wind Tunnel Testing, 3rd Edition, Wiley, 1999.

11 van Dam, C.P., Mayda, E.A., and Chao, D.D., "Computational Design and Analysis of Flatback Airfoil Wind Tunnel Experiment," SAND2008-1782, Sandia National Laboratories, Albuquerque, NM, March 2008.

Appendix

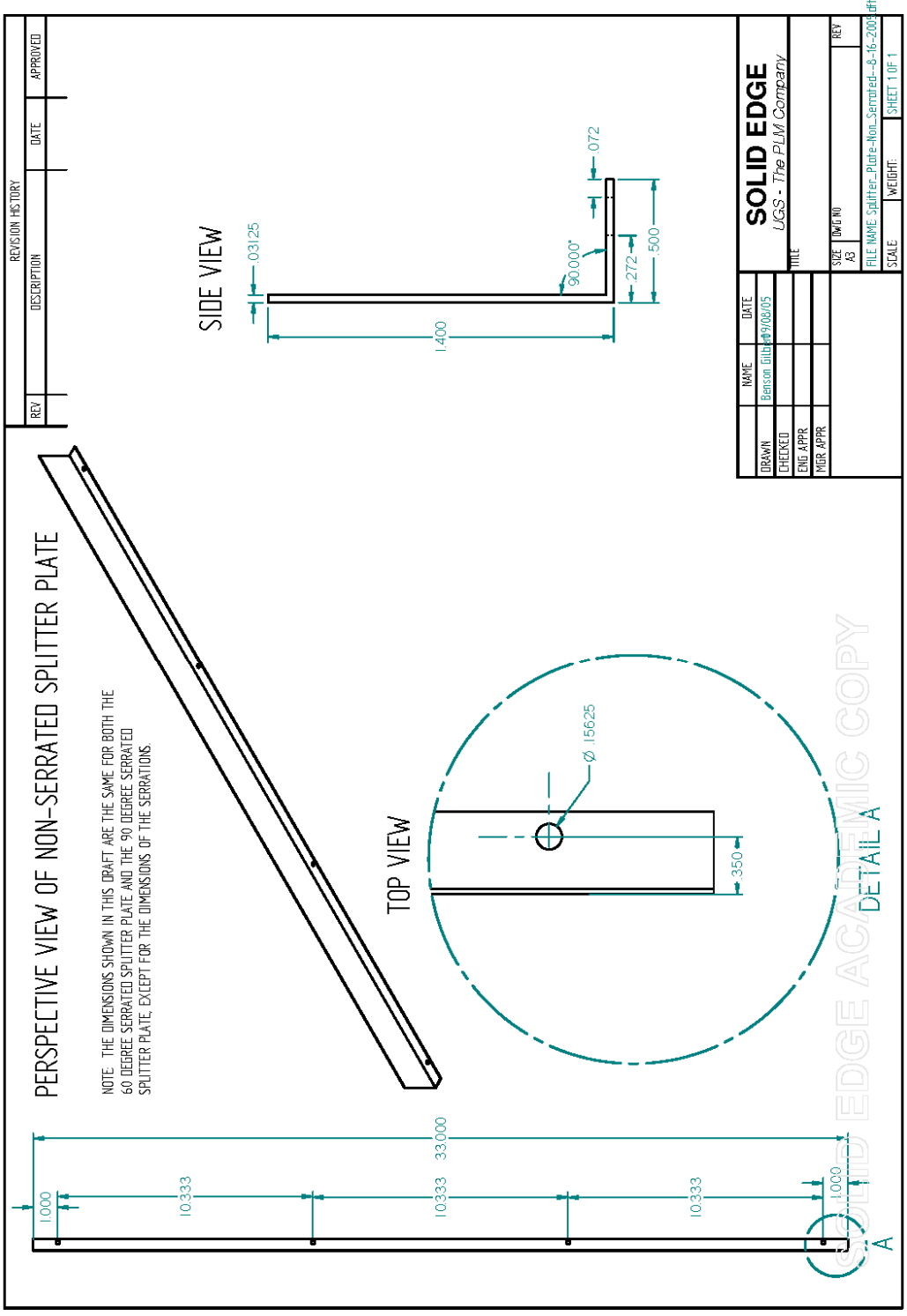

Figure A-1 Non-serrated splitter plate machine drawings.

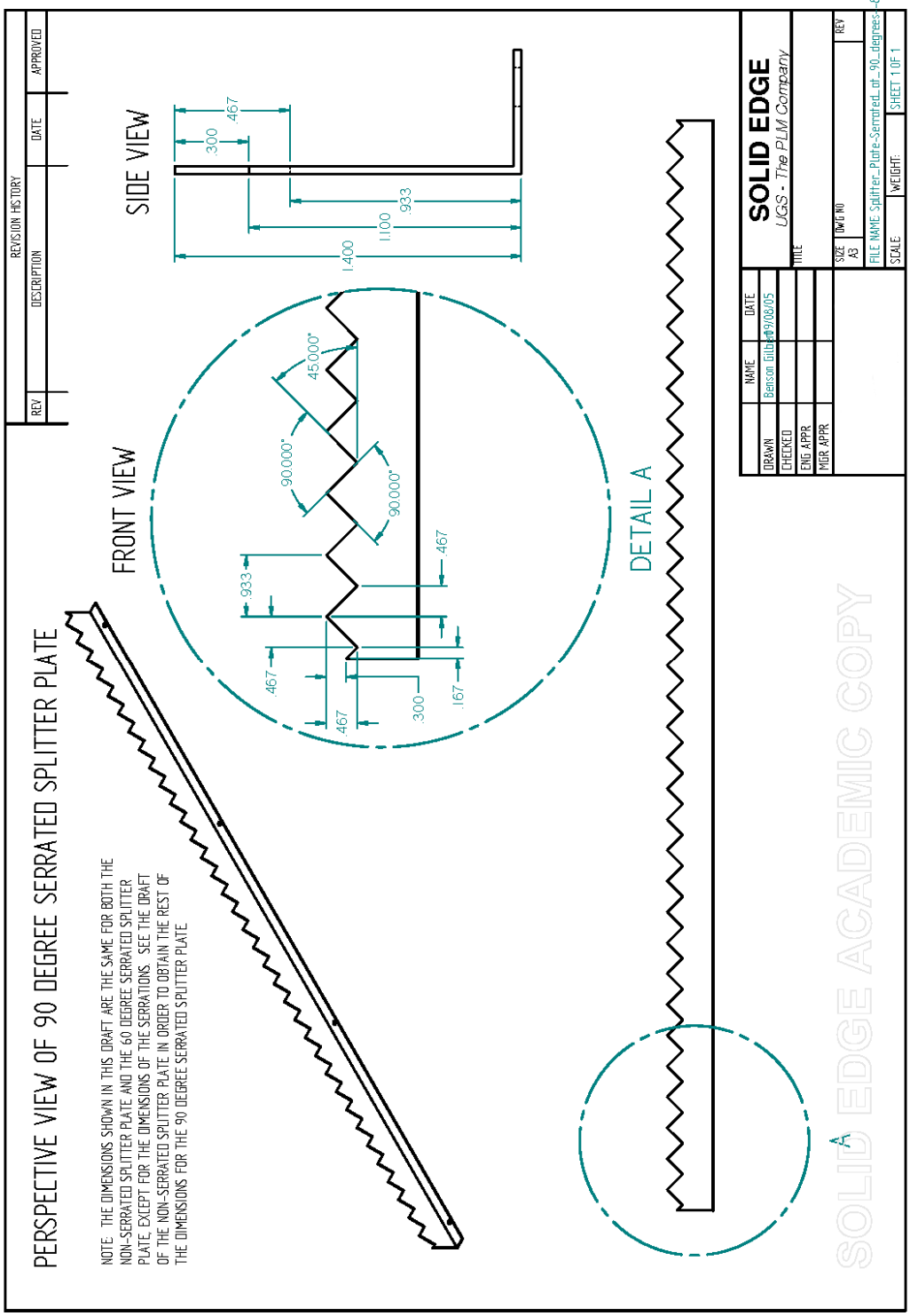

Figure A-2 90º-serrated splitter plate machine drawings.

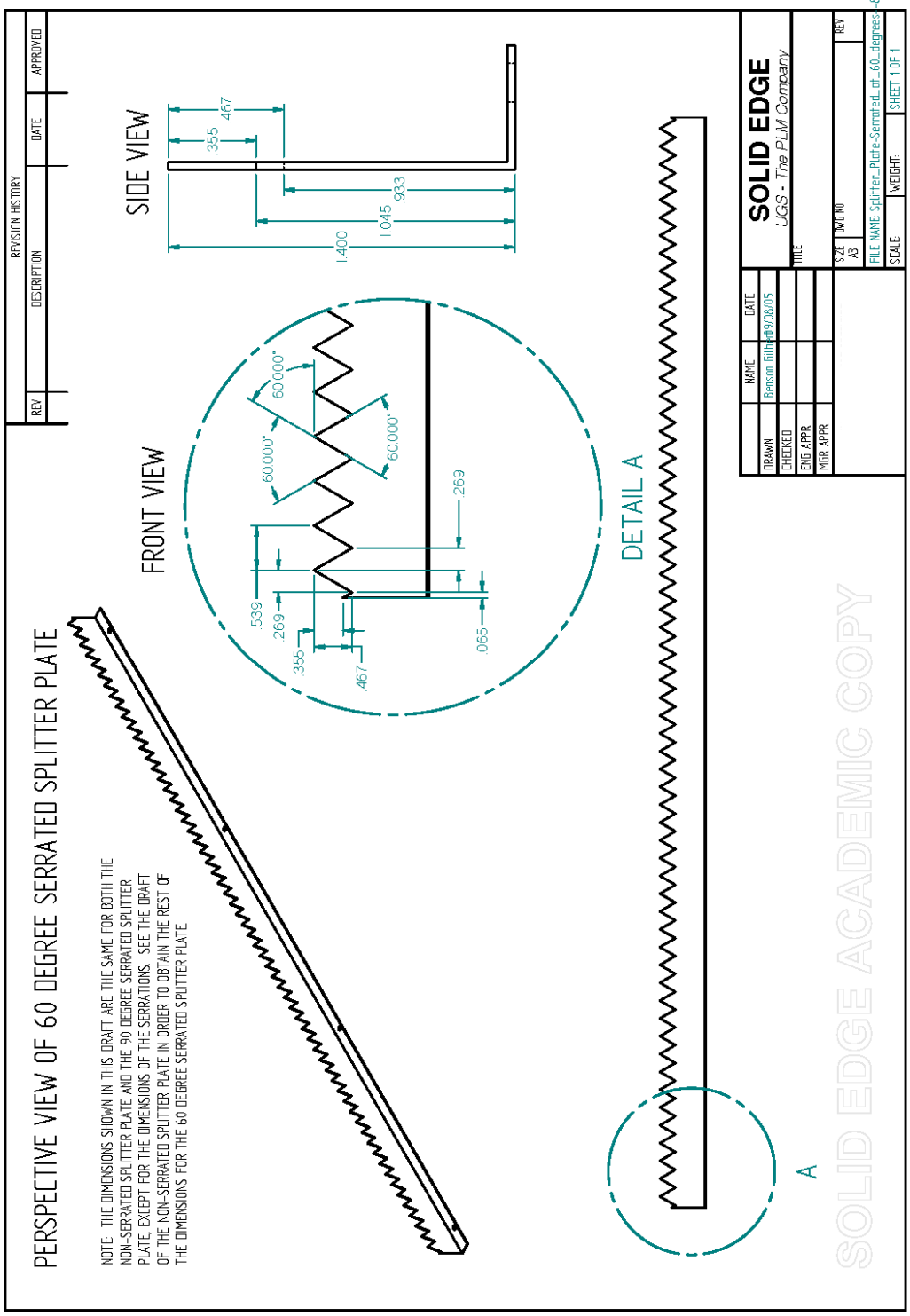

Figure A-3 60º-serrated splitter plate machine drawings.

DISTRIBUTION:

Tom Acker
Northern Arizona University
PO Box 15600
Flagstaff, AZ 86011-5600

Ian Baring-Gould
NREL/NWTC
1617 Cole Boulevard MS 3811
Golden, CO 80401

Keith Bennett
U.S. Department of Energy
Golden Field Office
1617 Cole Boulevard
Golden, CO 80401-3393

Karl Bergey
University of Oklahoma
Aerospace Engineering Dept.
Norman, OK 73069

Mike Bergey
Bergey Wind Power Company
2200 Industrial Blvd.
Norman, OK 73069

Derek Berry
TPI Composites, Inc.
373 Market Street
Warren, RI 02885-0328

Gunjit Bir
NREL/NWTC
1617 Cole Boulevard MS 3811
Golden, CO 80401

Marshall Buhl
NREL/NWTC
1617 Cole Boulevard MS 3811
Golden, CO 80401

C.P. Sandy Butterfield
NREL/NWTC
1617 Cole Boulevard MS 3811
Golden, CO 80401

Garrett Bywaters
Northern Power Systems
182 Mad River Park
Waitsfield, VT 05673

Doug Cairns
Montana State University
Dept. of Mechanical & Industrial Eng.
College of Engineering
PO Box 173800
Bozeman, MT 59717-3800

David Calley
Southwest Windpower
1801 West Route 66
Flagstaff, AZ 86001

Larry Carr
NASA Ames Research Center
24285 Summerhill Ave.
Los Altos, CA 94024

Jamie Chapman
Texas Tech University
Wind Science & Eng. Research Center
Box 41023
Lubbock, TX 79409-1023

Kip Cheney
PO Box 456
Middlebury, CT 06762

Craig Christensen
Clipper Windpower Technology, Inc.
6305 Carpinteria Ave. Suite 300
Carpinteria, CA 93013

R. Nolan Clark
USDA - Agricultural Research Service
PO Drawer 10
Bushland, TX 79012

C. Cohee
Foam Matrix, Inc.
1123 E. Redondo Blvd.
Inglewood, CA 90302

Joe Cohen
Princeton Economic Research, Inc.
1700 Rockville Pike, Suite 550
Rockville, MD 20852

C. Jito Coleman
Northern Power Systems
182 Mad River Park
Waitsfield, VT 05673

Ken J. Deering
The Wind Turbine Company
PO Box 40569
Bellevue, WA 98015-4569

James Dehlsen
Clipper Windpower Technology, Inc.
6305 Carpinteria Ave. Suite 300
Carpinteria, CA 93013

Edgar DeMeo
Renewable Energy Consulting Services
2791 Emerson St.
Palo Alto, CA 94306

S. Finn
GE Global Research
One Research Circle
Niskayuna, NY 12309

Peter Finnegan
GE Global Research
One Research Circle
Niskayuna, NY 12309

Trudy Forsyth
NREL/NWTC
1617 Cole Boulevard
Golden, CO 80401

Brian Glenn
Clipper Windpower Technology, Inc.
6305 Carpinteria Ave. Suite 300
Carpinteria, CA 93013

R. Gopalakrishnan
GE Wind Energy
GTTC, 300 Garlington Road
Greenville, SC 29602

Dayton Griffin
Global Energy Concepts, LLC
1809 7th Ave., Suite 900
Seattle, WA 98101

Maureen Hand
NREL/NWTC
1617 Cole Boulevard MS 3811
Golden, CO 80401

Thomas Hermann
Odonata Research
202 Russell Ave. S.
Minneapolis, MN 55405-1932

D. Hodges
Georgia Institute of Technology
270 Ferst Drive
Atlanta, GA 30332

William E. Holley
GE Wind Energy
GTTC, M/D 100D
300 Garlington Rd.
PO Box 648
Greenville, SC 29602-0648

Adam Holman
USDA - Agricultural Research Service
PO Drawer 10
Bushland, TX 79012-0010

D.M. Hoyt
NSE Composites
1101 N. Northlake Way, Suite 4
Seattle, WA 98103

Scott Hughes
NREL/NWTC
1617 Cole Boulevard MS 3911
Golden, CO 80401

Kevin Jackson
Dynamic Design
123 C Street
Davis, CA 95616

Eric Jacobsen
GE Wind Energy - GTTC
300 Garlington Rd.
Greenville, SC 29602

George James
Structures & Dynamics Branch
Mail Code ES2
NASA Johnson Space Center
2101 NASA Rd 1
Houston, TX 77058

Jason Jonkman
NREL/NWTC
1617 Cole Boulevard
Golden, CO 80401

Gary Kanaby
Knight & Carver Yacht Center
1313 Bay Marina Drive
National City, CA 91950

Benjamin Karlson
Wind Energy Technology Department
Room 5H-088
1000 Independence Ave. S.W.
Washington, DC 20585

Jason Kiddy
Aither Engineering, Inc.
4865 Walden Lane
Lanham, MD 20706

M. Kramer
Foam Matrix, Inc.
PO Box 6394
Malibu, CA 90264

David Laino
Windward Engineering
8219 Glen Arbor Dr.
Rosedale, MD 21237-3379

Scott Larwood
1120 N. Stockton St.
Stockton, CA 95203

Bill Leighty
Alaska Applied Sciences, Inc.
PO Box 20993
Juneau, AK 99802-0993

Wendy Lin
GE Global Research
One Research Circle
Niskayuna, NY 12309

Steve Lockard
TPI Composites, Inc.
373 Market Street
Warren, RI 02885-0367

James Locke
AIRBUS North America Eng., Inc.
213 Mead Street
Wichita, KS 67202

James Lyons
Novus Energy Partners
201 North Union St., Suite 350
Alexandria, VA 22314

David Malcolm
Global Energy Concepts, LLC
1809 7th Ave., Suite 900
Seattle, WA 98101

John F. Mandell
Montana State University
302 Cableigh Hall
Bozeman, MT 59717

Tim McCoy
Global Energy Concepts, LLC
1809 7th Ave., Suite 900
Seattle, WA 98101

L. McKittrick
Montana State University
Dept. of Mechanical & Industrial Eng.
220 Roberts Hall
Bozeman, MT 59717

Amir Mikhail
Clipper Windpower Technology, Inc.
6305 Carpinteria Ave. Suite 300
Carpinteria, CA 93013

Patrick Moriarty
NREL/NWTC
1617 Cole Boulevard
Golden, CO 80401

Walt Musial
NREL/NWTC
1617 Cole Boulevard MS 3811
Golden, CO 80401

Library (5) NWTC
NREL/NWTC
1617 Cole Boulevard
Golden, CO 80401

Byron Neal
USDA - Agricultural Research Service
PO Drawer 10
Bushland, TX 79012

Steve Nolet
TPI Composites, Inc.
373 Market Street
Warren, RI 02885-0328

Richard Osgood
NREL/NWTC
1617 Cole Boulevard
Golden, CO 80401

Tim Olsen
Tim Olsen Consulting
1428 S. Humboldt St.
Denver, CO 80210

Robert Z. Poore
Global Energy Concepts, LLC
1809 7th Ave., Suite 900
Seattle, WA 98101

Cecelia M. Poshedly (5)
Office of Wind & Hydropower Techologies
EE-2B Forrestal Building
U.S. Department of Energy
1000 Independence Ave. SW
Washington, DC 20585

Robert Preus
Abundant Renewable Energy
22700 NE Mountain Top Road
Newberg, OR 97132

Jim Richmond
MDEC
3368 Mountain Trail Ave.
Newberg Park, CA 91320

Michael Robinson
NREL/NWTC
1617 Cole Boulevard
Golden, CO 80401

Dan Sanchez
U.S. Department of Energy
NNSA/SSO
PO Box 5400 MS 0184
Albuquerque, NM 87185-0184

Scott Schreck
NREL/NWTC
1617 Cole Boulevard MS 3811
Golden, CO 80401

David Simms
NREL/NWTC
1617 Cole Boulevard MS 3811
Golden, CO 80401

Brian Smith
NREL/NWTC
1617 Cole Boulevard MS 3811
Golden, CO 80401

J. Sommer
Molded Fieber Glass Companies/West
9400 Holly Road
Adelanto, CA 92301

Ken Starcher
Alternative Energy Institute
West Texas A & M University
PO Box 248
Canyon, TX 79016

Fred Stoll
Webcore Technologies
8821 Washington Church Rd.
Miamisburg, OH 45342

Herbert J. Sutherland
HJS Consulting
1700 Camino Gusto NW
Albuquerque, NM 87107-2615

Andrew Swift
Texas Tech University
Civil Engineering
PO Box 41023
Lubbock, TX 79409-1023

J. Thompson
ATK Composite Structures
PO Box 160433 MS YC14
Clearfield, UT 84016-0433

Robert W. Thresher
NREL/NWTC
1617 Cole Boulevard MS 3811
Golden, CO 80401

Steve Tsai
Stanford University
Aeronautics & Astronautics
Durand Bldg. Room 381
Stanford, CA 94305-4035

William A. Vachon
W. A. Vachon & Associates
PO Box 149
Manchester, MA 01944

C.P. van Dam (10)
Dept. of Mechanical & Aerospace Eng.
University of California, Davis
One Shields Avenue
Davis, CA 95616-5294

Jeroen van Dam
Windward Engineering
NREL/NWTC
1617 Cole Boulevard
Golden, CO 80401

Brian Vick
USDA - Agricultural Research Service
PO Drawer 10
Bushland, TX 79012

Carl Weinberg
Weinberg & Associates
42 Green Oaks Court
Walnut Creek, CA 94596-5808

Kyle Wetzel
Wetzel Engineering, Inc.
PO Box 4153
Lawrence, KS 66046-1153

Mike Zuteck
MDZ Consulting
601 Clear Lake Road
Clear Lake Shores, TX 77565

INTERNAL DISTRIBUTION:

MS 0557 D.T. Griffith, 1524
MS1124 J.R. Zayas, 6333
MS 1124 T.D. Ashwill, 6333
MS 1124 M.E. Barone, 01515
MS 1124 D.E. Berg, 6333 (10)
MS 1124 S.M. Gershin, 6333
MS 1124 R.R. Hill, 6333
MS 1124 W. Johnson, 6333
MS 1124 D.L. Laird, 6333
MS 1124 D.W. Lobitz, 6333
MS 1124 J. Paquette, 6333
MS 1124 M.A. Rumsey, 6333
MS 1124 J. Stinebaugh, 6333
MS 1124 P.S. Veers, 6333
MS 0899 Technical Library, 9536
(Electronic)


Sandia National Laboratories